Impact of different metallic forms of nickel on hydrogen evolution reaction

Abhishek Lahiri[1*], Annu Kumar Lakshya[2], Shaoliang Guan[3,4], Lorna Anguilano[5], Anirban Chowdhury[2*]

[1]Department of Chemical Engineering, Brunel University London, Kingston lane, Uxbridge, UB8 3PH

[2]MAPS (Materials Process - Structure correlations) Laboratory, Metallurgical and Materials Engineering, Indian Institute of Technology Patna, Bihar, India

[3]School of Chemistry, Cardiff University, Cardiff CF10 3AT, United Kingdom

[4]HarwellXPS, Research Complex at Harwell, Rutherford Appleton Laboratory, Didcot OX11 0FA, United Kingdom

[5]Experimental Techniques Centre, College of Engineering, Design and Physical Science, Brunel University London, Kingston Lane, London UB8 3PH, UK

***Corresponding authors: abhishek.lahiri@brunel.ac.uk (A. Lahiri); anirban.chowdhury@gmail.com (A. Chowdhury)**

Abstract

In this work, we show the influence of strain in two different forms (plate and foil) of nickel for hydrogen evolution reaction (HER) in alkaline solution and 3.5% NaCl aqueous solution. The presence of tensile strain in nickel foil lowers the overpotential by about 10 mV to reach a current density of 10 mA cm^{-2} and improves the reaction kinetics of HER in alkaline solution. The Tafel slope showed a significant change in the strained nickel (i.e., in Ni foil) which gave a value of 111 mV dec^{-1} compared to unstrained nickel (Ni plate) which was found to be 151 mV dec^{-1}, thus indicating a change in reaction mechanism. Compared to alkaline solution, the effect of strain becomes less pronounced in NaCl solution which can be attributed to Cl^- adsorption on the electrode, thereby reducing its catalytic activity.

Keywords: Hydrogen evolution reaction; lattice strain; Nickel; Alkaline solution; Sea water

Hydrogen is one of the most explored option for a benign source of renewable energy at recent times [1]. Electrolysis of alkaline water provides one such convenient solution/s for producing hydrogen where water is electrochemically split into H_2 and O_2 with the help of a suitable electrode. Along with economic factors, low maintenance, enhanced durability and reliability are the prime reasons why Nickel (Ni) is popularly used at an industrial scale for the reduction of water [2, 3]. Surface reactivity plays an important role in heterogeneous electrocatalysis and depends on the crystal structure, surface electronic states and the number of active sites [4, 5]. These parameters can be tuned by inducing surface strain. Several recent studies have shown the effect of strain in nanoparticles that can improve various electrocatalytic processes [4-7]. Surface strain can be induced in the material through external forces, doping, dealloying, annealing, controlling the growth process (e.g., epitaxial growth) or through lattice mismatch [8-13]. For example, Voiry et al. [14] showed that chemically exfoliated WS_2 contained high concentration of strained metallic octahedral phase which resulted in improved hydrogen evolution. Strasser et al. [15] showed that the catalytic activity of PtCu@Cu corer-shell system (that was formed by de-alloying Pt–Cu nanoparticles) improved due to the elastic strain in the de-alloyed shell.

However, most studies have been limited to understand the strain effect in noble metal nanoparticles with the limited industrial prospect. Considerably, little is known about the effect of strain in thin films and its influence on catalytic properties. Yan et al. [12] systematically studied the effect of mechanical strain on Pt, Cu, and Ni films and its effect on hydrogen evolution reaction (HER) by combining experiment and theory. They showed that the catalytic activities of Ni and Pt thin films improved by compression, whereas in Cu thin films, tension was required to improve the catalytic activity. More recently, it was shown that on applying mechanical strain, the HER activity could be increased on Pd by reducing the hydrogen absorption properties in Pd [16]. Application of mechanical strain has also been reported to

induce lattice mismatch in atomically developed thin films, finally influencing the catalytic property [17].

Considering from an industrial perspective wherein nickel is used as cathodes for HER, we looked into the HER performance in commercially available nickel forms for hydrogen generation in alkaline and NaCl solution. The HER performances were recorded with two different commercially available metallic forms of nickel: annealed thick nickel plate and thin nickel foil. Surprising improvements in catalytic properties (in alkaline solution and 3.5wt% NaCl) were noted for Ni foil. A subsequent analysis was followed to find out the contributing factor for such an improved catalytic performance.

Fig. 1 compares the linear scan voltammetry (LSV) and Tafel plots of nickel plate and nickel foil in 1M NaOH and 3.5% NaCl at different temperatures. It is evident from Fig. 1(a) that HER of Ni foil in NaOH electrolyte occurs at lower overpotential compared to nickel plate. Table 1 compares the overpotential to reach a current density of 10 mA cm^{-2} for the nickel plate and nickel foil at different temperatures. Noteworthy that, at all temperatures, Ni foil shows a lower overpotential to attain 10 mA cm^{-2}. This is further confirmed by plotting the Tafel plots (Fig. 1(b)) wherein a Tafel slope of 111 mV dec^{-1} is obtained for Ni foil whereas an increase in Tafel slope of 151 mV dec^{-1} is obtained for Ni plate. Previous studies [18, 19] have shown that bare nickel exhibits a Tafel slope of greater than 120 mV dec^{-1} in 1M NaOH at 293 K, and therefore obtaining a value of 111 mV dec^{-1} indicates a possible lattice strain within the nickel foil that may be responsible for lowering the Tafel slope.

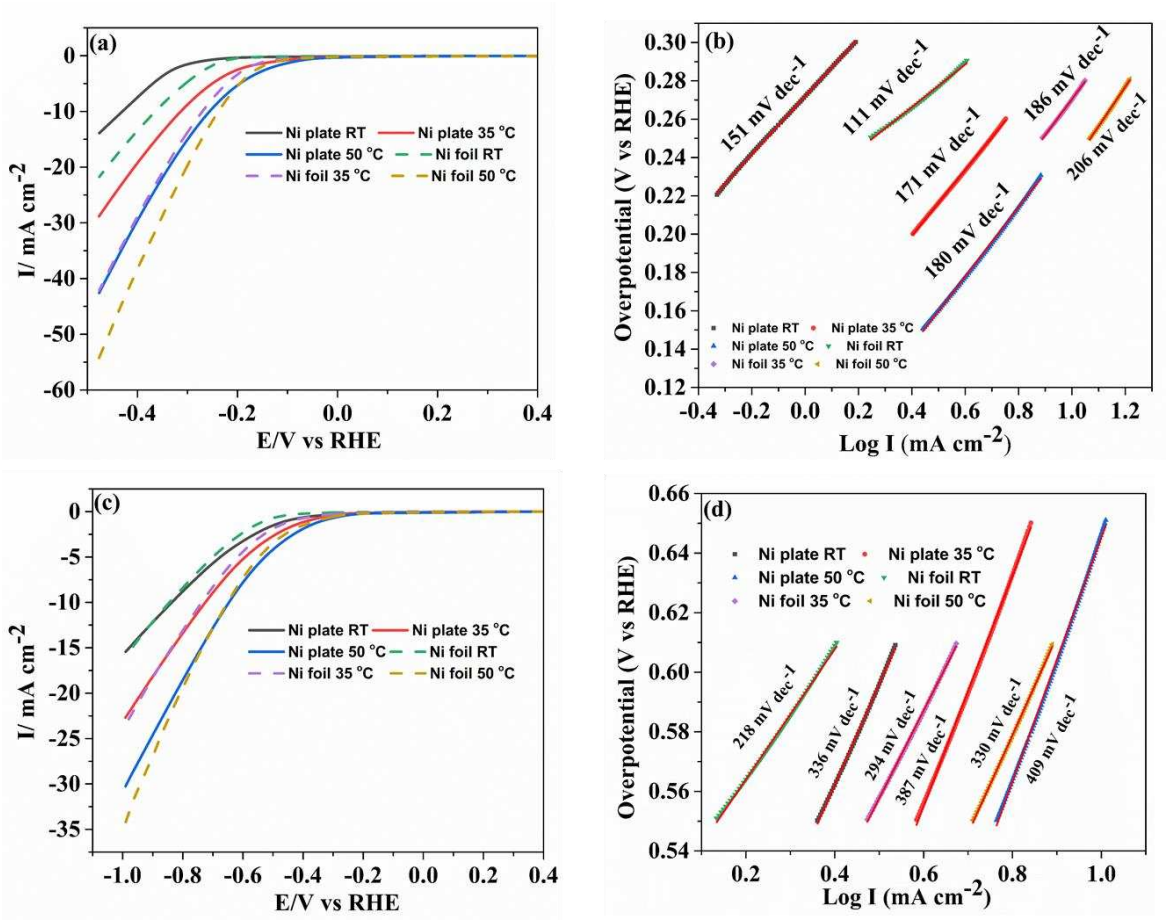

Fig. 1. (a) Linear scan voltammetry of nickel plate (solid lines) and nickel foil (dash lines) in 1M NaOH at different temperatures (b) Tafel plot of Ni plate and Ni foil in 1M NaOH (c) LSV of nickel plate (solid lines) and nickel foil (dash lines) in 3.5 wt% NaCl at different temperatures (d) Tafel plot of Ni plate and Ni foil in 3.5 wt% NaCl

Table 1

Kinetics parameters for the HER on Ni plate and Ni foam catalysts in 1 M NaOH and 3.5 wt% NaCl

Ni plate				Ni foil			
1M NaOH							
Temperature (K)	Overpotential at 10 mA cm^{-2}	Tafel slope mV dec^{-1}	Exchange current density mA cm^{-2}	Temperature (K)	Overpotential at 10 mA cm^{-2}	Tafel slope mV dec^{-1}	Exchange current density mA cm^{-2}
293	0.43 V	151	0.27	293	0.35 V	111	0.22
308	0.3 V	171	0.13	308	0.27 V	186	0.08
323	0.25 V	180	0.07	323	0.23 V	206	0.03
3.5 wt% NaCl							
293	0.83V	336	0.41	293	0.83	218	0.52
308	0.72V	387	0.32	308	0.73	294	0.41
323	0.64V	410	0.23	323	0.64	330	0.31

On changing the electrolyte from NaOH to NaCl, the HER process does not show a significant difference between the two Ni substrates at all temperatures (Fig. 1c). This can be ascribed to the adsorption of Cl ions on the nickel. However, on calculating the Tafel slope (Fig. 1(d), Table 1), a significant difference is observed wherein Ni foil shows a lower Tafel slope (by more than 100 mV dec^{-1}). This indicates that the reaction kinetics might be different on Cl adsorption. The durability of Ni foil and plate were tested by running constant current density experiments at 10 mA cm^{-2} for 30 hours (Fig. S1a). A stable potential was observed. The disturbance in the plot is due to hydrogen evolution at the Ni electrode. The HER performance of the catalyst after 30 hours showed slight increase in overpotential for both Ni plate and Ni foil (Fig. S1b, Fig. S1c). However, the magnitude of the overpotential on Ni foil was found to be considerably lower compared to the Ni plate. Furthermore, the electrochemical surface active area (ESCA) was determined using capacitive method (Fig. S2) from which it was evident that the active surface area of Ni foil is three (03) times higher than Ni plate which led to a change in reaction kinetics and lowering of overpotential.

To identify the improvement in reaction kinetics in HER and find a possible correlation (if any) with lattice strain in the nickel substrates, X-ray diffraction (XRD) and electron backscatter diffraction (EBSD) were performed.

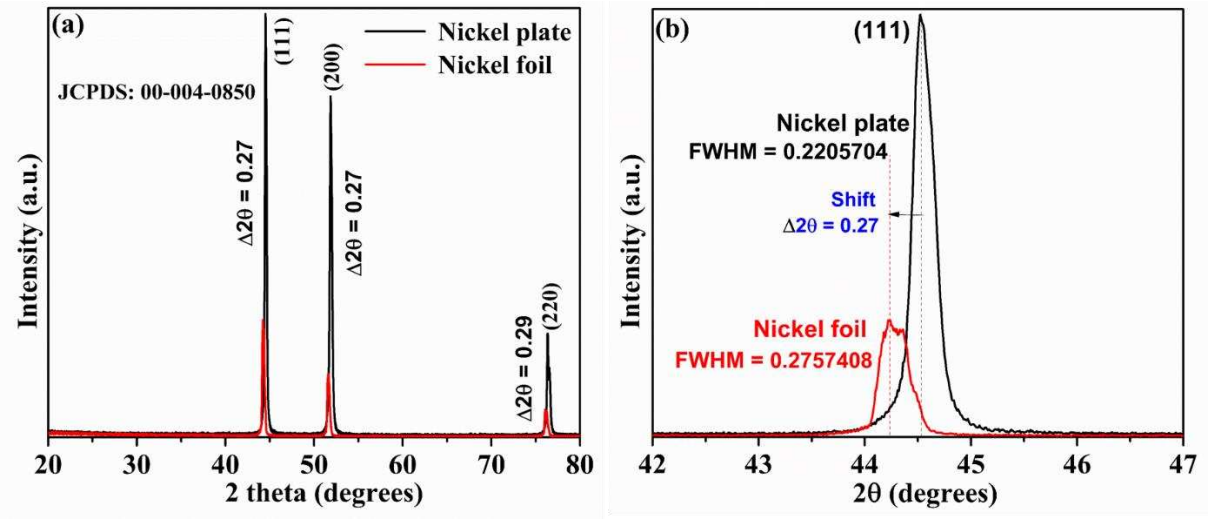

Fig. 2. (a) XRD plot for Nickel sample: plate and foil (b) magnified view of the (111) peak in XRD showing peak broadening and peak shift towards lower 2θ angle.

The XRD pattern of both nickel plate and foil, shown in Fig. 2(a), confirms a face-centered cubic symmetry for nickel (JCPDS file no. 4-0850) with no evidence of extra/new phases. All the XRD peaks of nickel foil were noted to shift to a lower angle and are broader as shown in Fig. 2(b). This peak shift indicates an increase in the lattice parameter and suggests the presence of tensile strain in nickel foil. The calculated full width at half maxima (FWHM) of both XRD peaks (of Ni) reveals that FWHM of nickel foil was approx. 125% higher than nickel plate. The fact that the peak shift (to a lower angle) occurred simultaneously with the broadening shows that the induced strain is large and may possibly due to a microstructural rearrangement on nickel foil. The same is confirmed from the grain size distributions as revealed from the EBSD analyses. For the given same area, massive grain refinement (i.e., the significant increase in number of grain boundaries) is noted for the nickel foil sample compared to the Ni plate

where mostly bigger grains (>50 μm) are noted, (as shown in supplementary Fig. S3- S6). In other words, the Ni plate may be taken as a 'strain relaxed' system owing to its bigger grains, while the smaller grains in the Ni foil contributed to more defects and strains in the overall matrix.

The lattice parameters calculated for the nickel plate from XRD data (from all three major reflections) was 3.5236 ± 0.0009 Å. It matches with the stated JCPDS file that portrays the lattice parameter value of 3.5238 Å. For the nickel foil, an increased lattice parameter was observed (3.5412 ± 0.0014 Å). As no doping was involved, the increased lattice parameter can be attributed to tensile strain within the foil. Various earlier results [20, 21] have also contributed the factor of increase in lattice parameter to tensile strain enhancements. Noteworthy that, possible important sources of strain in any metallic sample (e.g., Ni) may be due to a variety of factors, e.g., stacking faults, twinning, grain boundaries, sub boundaries, etc. [22]. However, we believe that with smaller grains (i.e., more number of grain boundaries), the in-plane tensile strain also contributed to the cause of peak shift. To separate individual contributions of stacking faults, twinning, grain boundary etc. for their roles on XRD peak shift and subsequently on the HER response may only be realised with in-depth future study. We have intentionally avoided the calculation of micro-strain (for Ni foil) via Williamson-Hall equation (W-H) as the grains in Ni foil are coupled with the strain factor that is coming from the neighborhood grain and, this would eventually lead to the wrong estimation of strain and size of grains [23]. The individual peak intensities of the metallic nickel samples were noted for a massive (> 350%) decrease; from nickel plate to the nickel foil sample. Such a huge decline in the peak intensities for the Ni foil sample once again indicate possible presence of various strain-induced defects. The lowering of overpotential can be ascribed to the residual tensile strain within the nickel foil along with difference in the grain size which improves the catalytic activity. A recent report has also suggested remarkable enhancements in catalytic

activities with increased grain boundary density [24]. This agrees with our studies for the case of Ni foil where smaller grains induce an in-plane tensile strain to portray enhanced HER responses.

Based on the d-band model, lattice strain causes an upshift in the d-band centre which improves the interaction with the adsorbate [6, 25, 26]. Therefore, in the case of nickel foil, it appears that there is good interaction between OH ions and the nickel surface which possibly reduces the overpotential required for HER. Based on the Tafel analysis, a Tafel slope of greater than 120 mV dec^{-1} clearly represents a Volmer step as the rate determining process for HER. However, theoretical studies have suggested that with high coverage of hydrogen atoms on the surface, Heyrovsky step also show a similar Tafel slope [27]. Therefore, in the case of Ni foil, the obtained slope of 111 mV dec^{-1} indicates that Heyrovsky step could be the kinetic controlled process for HER due to the presence of strain that leads to higher coverage of adsorbed hydrogen atoms. On increasing the temperature, a lowering of overpotential is observed (Fig. 1(a), Table 1) with an increase in Tafel slope and decrease in exchange current density (Fig. 1(b), Table 1). These changes could be related to the formation of a passive layer of NiOH/NiO on Ni substrate in 1M NaOH and is consistent with previous observations [18, 19, 28]. To further evaluate the influence of strain on interfacial processes of HER, impedance spectroscopy was performed at selected potentials on both Ni plate and Ni foil. Fig. 3 shows the impedance spectra of nickel foil and plate fitted with an Armstrong equivalent circuit. Clear difference in impedance spectra is observed and the values of the different elements are shown in supplementary Table S1. Table S1 clearly shows that the charge transfer resistance (R_{ct}) and double layer capacitance (C_{dl}) in Ni foil is lower than Ni plate close to the onset of hydrogen evolution reaction (125 mV). Furthermore, the sum of R_{ct} and pseudo-resistance (R_p) which represents the Faradaic resistance is also lower at 125 mV for Ni foil eventually resulting in higher kinetics of HER.

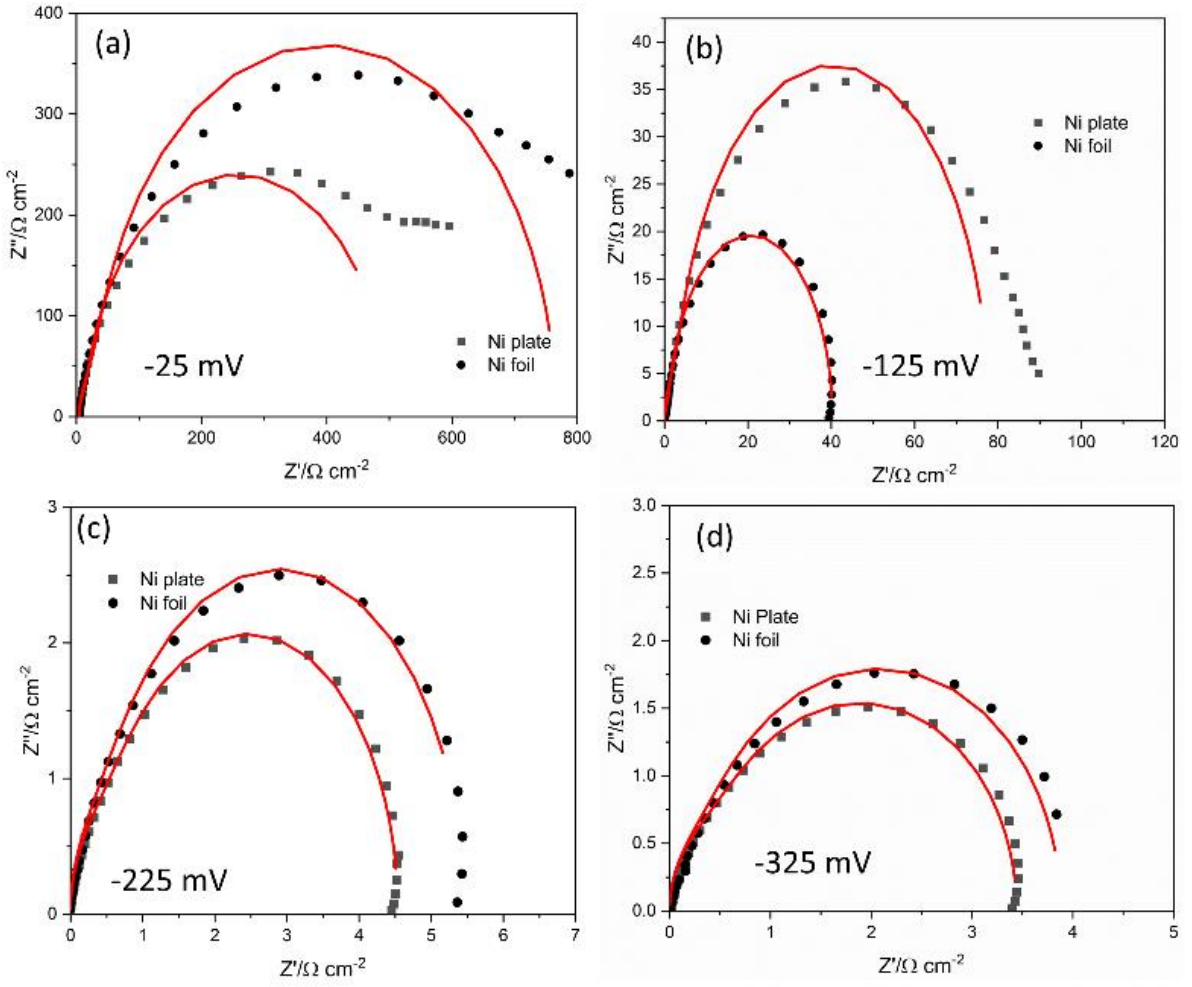

Fig. 3. Electrochemical impedance spectroscopy measurements conducted at various values of overpotential (a) -25 mV (b) -125 mV (c) -225 mV (d) -325 mV in 1M NaOH at 293 K

At higher overpotentials, R_{ct} for both nickel plate and nickel foil is similar whereas the double layer capacitance is lower for Ni foil. This suggests that a faster conversion of adsorbed hydrogen occurs on Ni foil which reduces to hydrogen. Thus, from the impedance measurements, it is apparent that the presence of strain in Ni foil clearly affects the interfacial processes to lower the overpotential of HER and also to improve the reaction kinetics of HER.

In order to confirm that strain increases the adsorption of ions, X-ray photoelectron spectroscopy was performed on the Ni foil and plate exposed to the electrolyte for 5 minutes

(Fig. 4). Fig. 4a compares the survey spectra of Ni foil and plate exposed to NaOH and NaCl electrolytes from which Ni, O, C and Cl peaks are observed. The C 1s peak arises from the impurity from air during sample transfer. Fig. 4b compares the high-resolution Ni 2p for the plate and foil exposed to 1M NaOH. Three major peaks related to $Ni2p_{3/2}$ are observed at 852.5 eV, 855.8 and 861.5 eV. The first two peaks correspond to metallic nickel and $Ni(OH)_2$ and the third broad peak relates to $Ni2p_{3/2}$ satellite. The broad peak above 870 eV corresponds to multiplet-split arising from NiO and $Ni(OH)_2$ [29]. On comparison of the $Ni2p_{3/2}$ at 852.5 eV it is evident that the intensity of metallic nickel has decreased considerably in Ni foil compared to Ni plate indicating a higher concentration of hydroxides on Ni foil due to strain contributions. The O1s spectra in Fig. 4c at 531 eV corresponds well with the formation of $Ni(OH)_2$ [30] and the additional deconvoluted peaks at 532.8 and 535.8 eV can be attributed to the presence of carbonate due to exposure of the sample in air. The high-resolution spectra of Na 1s and C 1s is shown in the supporting information (Fig. S7). Based on the XPS peak area, the Na concentration was found to be twice on Ni foil compared to that on Ni plate which confirms that adsorption of molecules on strained Ni surface is greater than the unstrained surface (of the Ni plate).

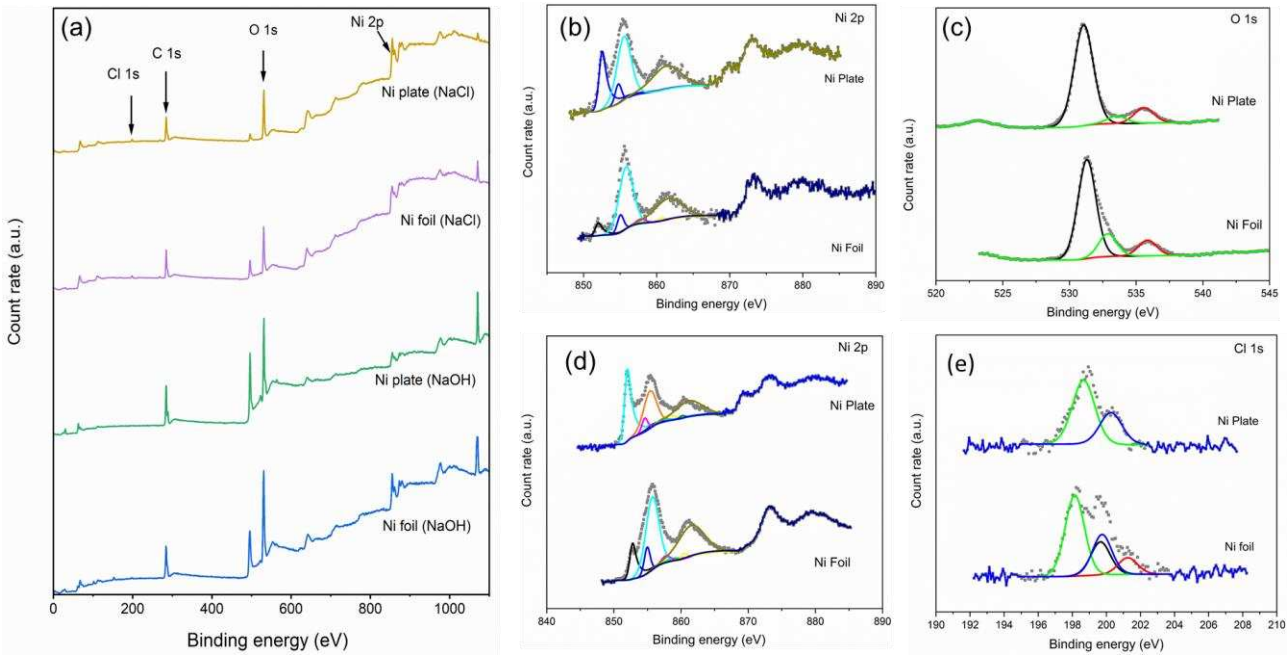

Fig. 4. (a) Comparison of XPS survey spectra of Ni plate and Ni foil spectra dipped in NaOH and NaCl electrolyte (b, c) Comparison of high-resolution Ni 2p and O1s spectra of nickel plate and foil dipped in NaOH (d, e) Comparison of high-resolution Ni 2p and Cl 1s spectra of nickel plate and foil dipped in NaCl

Similar observation is noted as Ni substrates were dipped in NaCl electrolyte. In Fig. 4d, the peak intensity of metallic nickel at 852.7 eV is much lower for Ni foil compared to Ni plate and the peak intensity of $NiCl_2/Ni(OH)_2$ at 855.7 eV (both peaks overlap) [31] is also high for the foil. The Cl 1s spectra in Fig. 4e shows a main peak and shoulder at 198.2 eV and 200.3 eV, respectively. The peak at 198.2 eV may be correlated to NaCl while the shoulder peak suggests the formation of $NiCl_2$. Clearly the peak intensity of $NiCl_2$ is high for Ni foil compared to Ni plate which might have changed the reaction kinetics as observed in Table 1. This is also consistent with the ESCA measurement which showed an increased in active surface area.

In summary, we have shown the significant impact of tensile strain (in nickel foils) that reduces the overpotential of HER in alkaline solution and increases its reaction kinetics. Tafel slope indicated that in strained nickel foils, Heyrovsky step could be the kinetic controlled process rather than Volmer step which is usually observed on nickel samples. Furthermore, impedance spectroscopy showed that charge transfer resistance is lower for strained nickel foils leading to an improved reaction kinetics for hydrogen evolution. Considering the fact that nickel is industrially used for water splitting reactions, our work indicates a new possible pathway where introduction of residual strains may lead to enhanced performances for these applications.

Acknowledgments

AL acknowledges Brunel Research Initiative and Enterprise Fund (BRIEF) for funding of the project. AKL is indebted to the financial support provided by Indian Institute of Technology Patna. The x-ray photoelectron (XPS) data collection was performed at the EPSRC National Facility for XPS ("HarwellXPS"), operated by Cardiff University and UCL, under Contract No. PR16195.

References

[1] J.O. Abe, A. Popoola, E. Ajenifuja, O. Popoola, International journal of hydrogen energy 44(29) (2019) 15072-15086.

[2] K. Zeng, D. Zhang, Progress in energy and combustion science 36(3) (2010) 307-326.

[3] D. Hall, Journal of the Electrochemical Society 128(4) (1981) 740.

[4] H. Mistry, A.S. Varela, S. Kühl, P. Strasser, B.R. Cuenya, Nature Reviews Materials 1(4) (2016) 1-14.

[5] H. Wang, S. Xu, C. Tsai, Y. Li, C. Liu, J. Zhao, Y. Liu, H. Yuan, F. Abild-Pedersen, F.B. Prinz, Science 354(6315) (2016) 1031-1036.

[6] M. Luo, S. Guo, Nature Reviews Materials 2(11) (2017) 1-13.

[7] J. Yao, W. Huang, W. Fang, M. Kuang, N. Jia, H. Ren, D. Liu, C. Lv, C. Liu, J. Xu, Small Methods 4(10) (2020) 2000494.

[8] V.A. Sethuraman, D. Vairavapandian, M.C. Lafouresse, T. Adit Maark, N. Karan, S. Sun, U. Bertocci, A.A. Peterson, G.R. Stafford, P.R. Guduru, The Journal of Physical Chemistry C 119(33) (2015) 19042-19052.

[9] J.R. Petrie, V.R. Cooper, J.W. Freeland, T.L. Meyer, Z. Zhang, D.A. Lutterman, H.N. Lee, Journal of the American Chemical Society 138(8) (2016) 2488-2491.

[10] L. Wang, Z. Zeng, W. Gao, T. Maxson, D. Raciti, M. Giroux, X. Pan, C. Wang, J. Greeley, Science 363(6429) (2019) 870-874.

[11] X. Wang, Y. Zhu, A. Vasileff, Y. Jiao, S. Chen, L. Song, B. Zheng, Y. Zheng, S.-Z. Qiao, ACS Energy Letters 3(5) (2018) 1198-1204.

[12] K. Yan, T.A. Maark, A. Khorshidi, V.A. Sethuraman, A.A. Peterson, P.R. Guduru, Angewandte Chemie 128(21) (2016) 6283-6289.

[13] J.R. Kitchin, J.K. Nørskov, M.A. Barteau, J. Chen, Physical review letters 93(15) (2004) 156801.

[14] D. Voiry, H. Yamaguchi, J. Li, R. Silva, D.C. Alves, T. Fujita, M. Chen, T. Asefa, V.B. Shenoy, G. Eda, Nature materials 12(9) (2013) 850-855.

[15] P. Strasser, S. Koh, T. Anniyev, J. Greeley, K. More, C. Yu, Z. Liu, S. Kaya, D. Nordlund, H. Ogasawara, Nature chemistry 2(6) (2010) 454-460.

[16] R.P. Jansonius, P.A. Schauer, D.J. Dvorak, B.P. MacLeod, D.K. Fork, C.P. Berlinguette, Angewandte Chemie International Edition 59(29) (2020) 12192-12198.

[17] I.A. Pasti, E. Fako, A.S. Dobrota, N. Lopez, N.V. Skorodumova, S.V. Mentus, ACS Catalysis 9(4) (2019) 3467-3481.

[18] E.A. Franceschini, G.I. Lacconi, H.R. Corti, Electrochimica Acta 159 (2015) 210-218.

[19] N. Krstajić, M. Popović, B. Grgur, M. Vojnović, D. Šepa, Journal of Electroanalytical Chemistry 512(1-2) (2001) 27-35.

[20] W. Li, Y. Zhao, Y. Liu, M. Sun, G.I. Waterhouse, B. Huang, K. Zhang, T. Zhang, S. Lu, Angewandte Chemie International Edition 60(6) (2021) 3290-3298.

[21] V. Darakchieva, M. Beckers, M.-Y. Xie, L. Hultman, B. Monemar, J.-F. Carlin, E. Feltin, M. Gonschorek, N. Grandjean, Journal of Applied Physics 103(10) (2008) 103513.

[22] T. Ungar, Scripta Materialia 51(8) (2004) 777-781.

[23] K. Kumar, A. Chowdhury, Handbook on Miniaturization in Analytical Chemistry, Elsevier2020, pp. 239-275.

[24] H.K. Park, H. Ahn, T.H. Lee, J.Y. Lee, M.G. Lee, S.A. Lee, J.W. Yang, S.J. Kim, S.H. Ahn, S.Y. Kim, Small methods 5(2) (2021) 2000755.

[25] B. Hammer, J.K. Nørskov, Surface science 343(3) (1995) 211-220.

[26] S. Schnur, A. Groß, Physical Review B 81(3) (2010) 033402.

[27] T. Shinagawa, A.T. Garcia-Esparza, K. Takanabe, Scientific reports 5(1) (2015) 1-21.

[28] B. Conway, L. Bai, International journal of hydrogen energy 11(8) (1986) 533-540.

[29] A.P. Grosvenor, M.C. Biesinger, R.S.C. Smart, N.S. McIntyre, Surface Science 600(9) (2006) 1771-1779.

[30] T. Zhou, Z. Cao, P. Zhang, H. Ma, Z. Gao, H. Wang, Y. Lu, J. He, Y. Zhao, Scientific reports 7(1) (2017) 1-9.

[31] C.D. Jones, A.R. Lewis, D.R. Jones, C.J. Ottley, K. Liu, J.W. Steed, Chemical science 11(28) (2020) 7501-7510.